J. Fluid Mech. (1992), *vol.* 242, *pp.* 701–720
Printed in Great Britain

Receptivity of a laminar boundary layer to the interaction of a three-dimensional roughness element with time-harmonic free-stream disturbances

By M. TADJFAR[1] AND R. J. BODONYI[2]

[1] MCAT Institute, Fluid Mechanics Laboratory, NASA Ames Research Center, Mail Stop 260-1, Moffett Field, CA 94035, USA

[2] Department of Aeronautical and Astronautical Engineering, The Ohio State University, 2036 Neil Ave. Mall, Columbus, OH 43210, USA

(Received 14 September 1991 and in revised form 13 March 1992)

Receptivity of a laminar boundary layer to the interaction of time-harmonic free-stream disturbances with a three-dimensional roughness element is studied. The three-dimensional nonlinear triple-deck equations are solved numerically to provide the basic steady-state motion. At high Reynolds numbers, the governing equations for the unsteady motion are the unsteady linearized three-dimensional triple-deck equations. These equations can only be solved numerically. In the absence of any roughness element, the free-stream disturbances, to the first order, produce the classical Stokes flow, in the thin Stokes layer near the wall (on the order of our lower deck). However, with the introduction of a small three-dimensional roughness element, the interaction between the hump and the Stokes flow introduces a spectrum of all spatial disturbances inside the boundary layer. For supercritical values of the scaled Strouhal number, $S_0 > 2$, these Tollmien–Schlichting waves are amplified in a wedge-shaped region, 15° to 18° to the basic-flow direction, extending downstream of the hump. The amplification rate approaches a value slightly higher than that of two-dimensional Tollmien–Schlichting waves, as calculated by the linearized analysis, far downstream of the roughness element.

1. Introduction

Boundary-layer transition has been one of the most active areas of research in fluid mechanics. Two types of transition are generally considered. The first type, bypass transition, is the process in which the external disturbances: sound, free-stream turbulence etc. or the internal disturbances: vibrations, roughness, etc. are strong enough that vortex stretching and other nonlinear mechanisms directly lead to turbulence without going through the known instability mechanisms. The second type is the so-called 'quiet' environment transition which evolves gradually, as has been experimentally documented, and can be followed by theory and numerical computations (see Reshotko 1976 and Mack 1984).

The latter type is broken down into four stages of development (Herbert & Bodonyi 1989): (1) receptivity; (2) primary instability; (3) secondary instability; (4) breakdown.

Most of the work in boundary-layer stability theory has been on the behaviour of the individual normal-mode solutions of the linearized, parallel stability equations.

Numerous methods have been suggested to calculate the neutral stability curves and growth rates of these normal modes. Even the widely used e^N method is based on the amplitude ratio of the most unstable mode of the linear theory. However, in natural transition a spectrum of instability waves is present and the boundary layers found in practice are not parallel. The local Reynolds number is constantly changing and the energy is being redistributed by the interaction of all the modes. This has brought the attention of experimental investigations to the evolution of wave packets in the boundary layer (see Gaster 1975, 1985; Gaster & Grant 1975; Gilev, Kachanov & Kozlov 1981; Kachanov 1985 and Mack & Kendall 1983). Gaster (1985) found that even very weak wave packets, with velocity fluctuations of the order of 5×10^{-4} when normalized by the free-stream velocity, are influenced by the non-parallel and nonlinear effects. Theoretical study of the wave packets has been slow owing to the complexity of the numerical computations.

Receptivity is the means by which a particular forced disturbance enters the boundary layer and initiates the transition process. If the initial disturbances are sufficiently large, they can grow by forcing mechanisms to nonlinear levels and eventually lead to turbulence (transition of the first type) and, therefore, bypass the well-known mechanisms of the second type. If they are small, they will tend to excite free disturbances in the boundary layer which are better known as Tollmien–Schlichting (T–S) waves. These waves will go through other stages of development depending on the nature of the problem. It is this first stage in the transition process which is the subject of this study.

Receptivity is fundamentally different from the classical eigenvalue stability problem. It is a boundary-value problem, since it involves the response of the boundary layer to an externally imposed disturbance. However, naturally occurring free-stream disturbances travel at much higher speeds than instability waves. Therefore, characteristic wavelengths of the free-stream disturbances at a given frequency are much longer than the T–S waves. Hence, a wavelength conversion is required to transfer energy from these long waves to the much shorter T–S waves. This wavelength conversion is the core of the receptivity problem (see Reshotko 1984). Goldstein (1983, 1985), Goldstein & Hultgren (1987, 1989) using asymptotic methods showed that the wavelength conversion takes place at locations where the mean flow exhibits rapid changes and non-parallel effects are important. Examples are near the leading edge of a body and/or any region downstream where locally the boundary layer has to adjust rapidly to local pressure gradients (roughness, blowing, etc.).

Here we are interested in the interaction of small protuberances (on the scale of the T–S wavelengths) in the surface geometry and unsteady free-stream disturbances. Using the triple-deck scaling of Stewartson & Williams (1969) and Smith (1979), Goldstein (1985) showed that small two-dimensional surface variations can produce a large coupling between T–S waves and the imposed disturbance, when these variations are sufficiently rapid (order of a T–S wavelength). However, Goldstein (1985) uses the linearized solution of Stewartson for the steady flow and his entire analysis is limited to the linearized case of a very small hump.

Recently, Bodonyi *et al.* (1989) have considered a numerical study of the interaction of free-stream disturbances and a small two-dimensional roughness element placed on a flat plate. In that study the two-dimensional nonlinear viscous–inviscid triple-deck equations were solved numerically to provide the basic steady motion. It was shown that the unsteady motion is governed by the unsteady linearized triple-deck equations, in suitably scaled variables. The solution was

assumed to be harmonic in time. Numerical solutions were found for a range of values of frequency of the imposed free-stream disturbances and the hump height. It was found that the amplitude of all disturbance quantities grows without bound, downstream of the hump, if $S_0 > 2.29\ldots$, where S_0 is the scaled Strouhal number based on the frequency of the free-stream disturbances. For values of $S_0 < 2.29\ldots$, the disturbances eventually decay to zero amplitude and the flow remains stable. Thus the numerical solutions illustrate the growth or decay of the T–S waves generated by the interaction between the free-stream disturbance and the two-dimensional roughness element, depending on the value of the scaled Strouhal number.

In this study, the analysis of Bodonyi *et al.* (1989) is extended to the interaction of a three-dimensional protuberance and time-harmonic disturbances in the free stream. The three-dimensional nonlinear triple-deck equations are solved numerically to provide the basic steady-state motion. It is shown that the governing equations for the unsteady motion are the unsteady linearized three-dimensional triple-deck equations. These equations can only be solved numerically. The interaction of free-stream disturbances with the local pressure gradients induced by the hump's presence introduces a spectrum of all spatial disturbances in the boundary layer. These disturbances travel downstream in the growing boundary layer and amplify or decay while interacting with each other. Again it is found that the growth or decay of T–S waves is dependent on the scaled Strouhal number. However, the three-dimensionality manifests itself in spanwise wavelength selection and modulation. It is also found that the growth of T–S waves is confined to a wedge-shaped region downstream of the roughness element.

2. Problem formulation

We shall consider the receptivity of a laminar boundary layer on a flat plate to the interaction of a small three-dimensional wall roughness element with free-stream time-harmonic disturbances. A small three-dimensional protuberance, of the order of the triple-deck structure (explained below), is placed at a distance L^* from the leading edge on an otherwise flat plate. The flow is assumed to be incompressible with a uniform free-stream equation plus a small time-harmonic oscillation of frequency ω imposed at infinity: $u^* = U^*_\infty[1+\delta\,\mathrm{e}^{-\mathrm{i}\omega t^*}]$; where $\delta \ll 1$. Consider a Cartesian coordinate system (x, y, z), non-dimensionalized by length L^*, with x in the streamwise direction, y in the spanwise direction, and z in the vertical direction with the origin taken at the leading edge. Also, time t is non-dimensionalized by the frequency ω.

The triple-deck structure is the asymptotic distinguished limit of the Navier–Stokes equations describing a small local flow structure, smaller than order one, in the boundary layer of an external flow at high Reynolds number (see figure 1). This flow structure could be caused by wall suction, slot injection, wall turning, etc. or in our problem by a small three-dimensional wall roughness. The Reynolds number is defined as:

$$Re = U^*_\infty L^*/\nu, \tag{2.1}$$

where ν is the kinematic viscosity of the fluid. This structure was discovered by Stewartson & Williams (1969) and also, independently, by Messiter (1970) and by Neiland (1969). Over the past twenty years it has found many applications in steady and unsteady flows (see Stewartson 1974 and Smith 1982, 1986).

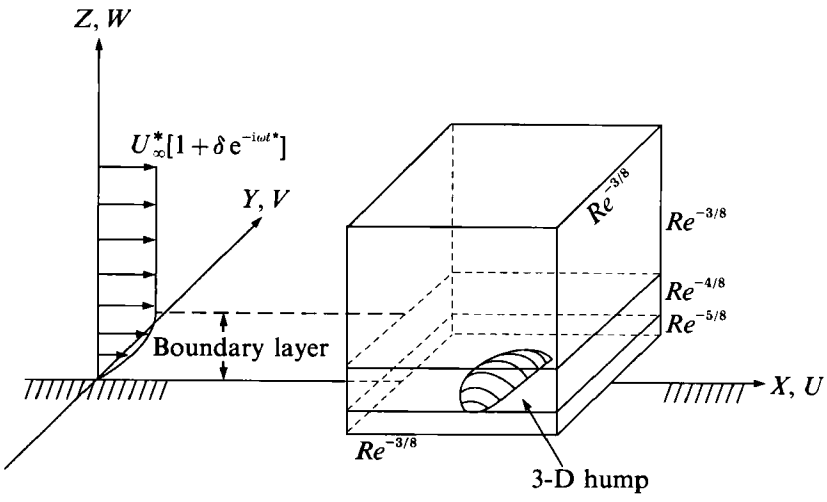

FIGURE 1. The triple-deck flow structure.

Assuming $Re \gg 1$, we define the small parameter ϵ:

$$\epsilon = Re^{-\frac{1}{8}}. \tag{2.2}$$

We wish to consider small humps of size $O(\epsilon^3 L^*)$ in the streamwise and spanwise directions (order of a T–S wavelength) and height $O(\epsilon^5 L^*)$. Thus, we define the rescaled independent variables (superscript * indicates dimensional variables):

$$(x, y) = \epsilon^{-3}\frac{(x^* - L^*, y^*)}{L^*}, \quad t = \omega t^*, \tag{2.3}$$

$$z_l = \epsilon^{-5} z^*/L^* \text{ in the lower deck}, \tag{2.4}$$

$$z_m = \epsilon^{-4} z^*/L^* \text{ in the main deck}, \tag{2.5}$$

$$z_u = \epsilon^{-3} z^*/L^* \text{ in the upper deck}. \tag{2.6}$$

The total flow quantities can be written as a steady flow part plus a small unsteady perturbation of $O(\delta)$:

$$V_F(\boldsymbol{x}, t) = V(\boldsymbol{x}) + \delta v(\boldsymbol{x}, t), \tag{2.7}$$

$$P_F(\boldsymbol{x}, t) = P(\boldsymbol{x}) + \delta p(\boldsymbol{x}, t). \tag{2.8}$$

Furthermore, the Navier–Stokes equations for an incompressible flow are written as

$$\nabla \cdot V_F = 0, \tag{2.9}$$

$$S\partial_t V_F + V_F \cdot \nabla V_F = -\nabla P_F + Re^{-1}\nabla^2 V_F, \tag{2.10}$$

where S is the Strouhal number defined by

$$S = \omega L^*/U_\infty^*. \tag{2.11}$$

Thus substituting (2.7) and (2.8) into the Navier–Stokes equations we have

$$\nabla \cdot V + \delta \nabla \cdot \boldsymbol{v} = 0, \tag{2.12}$$

and

$$V \cdot \nabla V + \nabla P - Re^{-1}\nabla^2 V + \delta\{S\partial_t \boldsymbol{v} + \boldsymbol{v} \cdot \nabla V + V \cdot \nabla \boldsymbol{v} + \nabla p - Re^{-1}\nabla^2 \boldsymbol{v}\} + \delta^2\{\boldsymbol{v} \cdot \nabla \boldsymbol{v}\} = 0. \tag{2.13}$$

The steady-state motion satisfies the Navier–Stokes equations to the 'zeroth' order:

$$\nabla \cdot V = 0, \tag{2.14}$$

$$V \cdot \nabla V = -\nabla P + Re^{-1}\nabla^2 V. \tag{2.15}$$

Subtracting (2.14) and (2.15) from (2.12) and (2.13), respectively, and neglecting the second-order terms in δ, we obtain the linearized Navier–Stokes equations governing the unsteady motion of the perturbed flow:

$$\nabla\cdot\boldsymbol{v}=0, \tag{2.16}$$

$$S\partial_t\boldsymbol{v}+\boldsymbol{v}\cdot\nabla\boldsymbol{V}+\boldsymbol{V}\cdot\nabla\boldsymbol{v}=-\nabla p+Re^{-1}\nabla^2\boldsymbol{v}. \tag{2.17}$$

2.1 *Basic steady-state flow*

As shown in previous steady triple-deck analyses the fundamental problem reduces to a consideration of the lower- and upper-deck equations. We shall solve the governing equations in both upper and lower decks simultaneously, subject to appropriate boundary and matching conditions. The appropriately scaled variables in the lower deck for the steady flow are

$$U(x,y,z_1)=\epsilon U_1(x,y,z_1)+O(\epsilon^2), \tag{2.18}$$

$$V(x,y,z_1)=\epsilon V_1(x,y,z_1)+O(\epsilon^2), \tag{2.19}$$

$$W(x,y,z_1)=\epsilon^3 W_1(x,y,z_1)+O(\epsilon^4), \tag{2.20}$$

$$P(x,y,z_1)=\epsilon^2 P_1(x,y,z_1)+O(\epsilon^3), \tag{2.21}$$

and the governing equations in the lower deck are the three-dimensional boundary-layer equations

$$\partial_x U_1+\partial_y V_1+\partial_{z_1} W_1=0, \tag{2.22}$$

$$U_1\partial_x U_1+V_1\partial_y U_1+W_1\partial_{z_1}U_1=-\partial_x P_1+\partial_{z_1z_1}U_1, \tag{2.23}$$

$$U_1\partial_x V_1+V_1\partial_y V_1+W_1\partial_{z_1}V_1=-\partial_y P_1+\partial_{z_1z_1}V_1, \tag{2.24}$$

$$P_1=P_1(x,y)\text{ only}, \tag{2.25}$$

subject to the boundary conditions

$$U_1=V_1=W_1=0\quad\text{on}\quad z_1=hF(x,y), \tag{2.26}$$

$$U_1\to\lambda z_1,\quad V_1,W_1,P_1\to 0\quad\text{as}\quad x\to-\infty\text{ and/or }y\to\pm\infty, \tag{2.27}$$

$$U_1\to\lambda(z_1+A(x,y))\quad\text{as}\quad z_1\to\infty, \tag{2.28}$$

$$\partial_x V_1\to-\frac{\partial_y P_1(x,y)}{\lambda z_1}\quad\text{as}\quad z_1\to\infty, \tag{2.29}$$

where $\lambda\equiv U_{\mathrm{B}}'(0)$ is the slope of the incoming velocity profile at the wall, $F(x,y)$ is the scaled order-one hump shape, and h is an order-one scaling parameter (with respect to the lower deck). $A(x,y)$ is the negative of the boundary-layer displacement thickness, and it is defined by asymptotic matching of all three decks.

The main deck (or middle layer) is simply a streamwise continuation of the upstream boundary layer. To first order, viscous forces are insignificant, and the governing equations can be solved analytically. This solution can be expressed physically as a simple transverse shift of the undisturbed boundary-layer flow. From the steady-state solution in the main deck we have:

$$U(\boldsymbol{x}_{\mathrm{m}})=U_{\mathrm{B}}(z_{\mathrm{m}})+\epsilon A(x,y)\,U_{\mathrm{B}}'+O(\epsilon^2), \tag{2.30}$$

$$V(\boldsymbol{x}_{\mathrm{m}})=\epsilon^2\frac{D(x,y)}{U_{\mathrm{B}}}+O(\epsilon^3), \tag{2.31}$$

$$W(\boldsymbol{x}_{\mathrm{m}})=-\epsilon^2\partial_x A(x,y)\,U_{\mathrm{B}}+O(\epsilon^3), \tag{2.32}$$

$$P(\boldsymbol{x}_{\mathrm{m}})=\epsilon^2 P_1(x,y)+O(\epsilon^3), \tag{2.33}$$

where $U_B(z_m)$ is the velocity profile of the incoming Blasius boundary layer and $D(x,y)$ is given by

$$D(x,y) = -\int_{-\infty}^{x} \partial_y P_1(\xi,y)\,\mathrm{d}\xi. \tag{2.34}$$

Equations (2.30)–(2.33) are coupled to the governing equations in the upper deck. The flow variables are appropriately scaled in the upper deck as

$$U(x,y,z_u) = 1+\epsilon^2\hat{U}_1(x,y,z_u)+O(\epsilon^3), \tag{2.35}$$

$$V(x,y,z_u) = \epsilon^2\hat{V}_1(x,y,z_u)+O(\epsilon^3), \tag{2.36}$$

$$W(x,y,z_u) = \epsilon^2\hat{W}_1(x,y,z_u)+O(\epsilon^3), \tag{2.37}$$

$$P(x,y,z_u) = \epsilon^2\hat{P}_1(x,y,z_u)+O(\epsilon^3). \tag{2.38}$$

It can be shown that the upper-deck problem reduces to a consideration of the Laplace equation for the steady pressure:

$$\nabla^2\hat{P}_1(x,y,z_u) = 0, \tag{2.39}$$

subject to the following boundary conditions:

$$\hat{P}_1 \to 0 \quad \text{as} \quad x\to-\infty, \tag{2.40}$$

$$\hat{P}_1 \to 0 \quad \text{as} \quad y\to\pm\infty, \tag{2.41}$$

$$\hat{P}_1 \to 0 \quad \text{as} \quad z_u\to\infty, \tag{2.42}$$

$$\partial_x\hat{P}_1 \to 0 \quad \text{as} \quad x\to\infty. \tag{2.43}$$

Also, matching between the upper and main decks requires that

$$\hat{P}_1(x,y,z_u\to 0) = P_1(x,y), \tag{2.44}$$

and

$$\partial_{z_u}\hat{P}_1(x,y,z_u\to 0) = \partial_{xx}A(x,y). \tag{2.45}$$

The above coupled equations with the given boundary and matching conditions present a well-posed problem. The nonlinear three-dimensional viscous–inviscid interaction problem given above can only be solved numerically for finite, order-one values of h.

2.2. *Receptivity problem*

The receptivity problem of the interaction between free-stream time-harmonic disturbances and a three-dimensional hump has the triple-deck structure as long as the hump height is of the order of the lower-deck thickness, $O(\epsilon^5)$. Furthermore, we are only interested in relatively high-frequency free-stream disturbances, therefore, we choose $S = O(\epsilon^{-2})$. This is of the same order as the Tollmien–Schlichting wave frequency at and upstream of the lower branch of the neutral stability curve. Thus we define a scaled Strouhal number S_0 such that:

$$S_0 = \epsilon^2 S. \tag{2.46}$$

As noted above, we are looking for solutions that are harmonic in time, since the problem is linear and our forcing free-stream disturbances are given as such. Therefore, we may write for our perturbation properties:

$$\boldsymbol{v}(\boldsymbol{x},t) = \mathrm{Re}\{\mathrm{e}^{-\mathrm{i}t}\,\boldsymbol{v}_c(\boldsymbol{x})\}, \tag{2.47}$$

$$p(\boldsymbol{x},t) = \mathrm{Re}\{\mathrm{e}^{-\mathrm{i}t}\,p_c(\boldsymbol{x})\}. \tag{2.48}$$

For convenience, the subscript c is dropped and all the perturbation-flow properties are assumed to be complex. Like the steady-state flow, the fundamental problem reduces to a consideration of the lower- and upper-deck equations (see Tadjfar 1990 for the details). In the lower deck, where $z \propto \epsilon^5$, the expansions for flow properties may be written as

$$u(x, y, z_1) = u_0(x, y, z_1) + O(\epsilon), \tag{2.49}$$

$$v(x, y, z_1) = v_0(x, y, z_1) + O(\epsilon), \tag{2.50}$$

$$w(x, y, z_1) = \epsilon^2 w_0(x, y, z_1) + O(\epsilon^3), \tag{2.51}$$

$$p(x, y, z_1) = \epsilon p_0(x, y, z_1) + O(\epsilon^2). \tag{2.52}$$

Similarly, in the upper deck, where $z \propto \epsilon^3$, the expansions for flow properties are

$$u(x, y, z_u) = 1 + \epsilon \hat{u}_1(x, y, z_u) + O(\epsilon^2), \tag{2.53}$$

$$v(x, y, z_u) = \epsilon \hat{v}_1(x, y, z_u) + O(\epsilon^2), \tag{2.54}$$

$$w(x, y, z_u) = \epsilon \hat{w}_1(x, y, z_u) + O(\epsilon^2), \tag{2.55}$$

$$p(x, y, z_u) = \epsilon \hat{p}_1(x, y, z_u) + O(\epsilon^2). \tag{2.56}$$

Putting the above expansions into (2.16) and (2.17), we obtain the governing equations pertinent to this problem. Here, we apply the Prandtl transposition theorem (see Rosenhead 1963, chap. 5, part 2, §8) to transform our computational domain in the lower deck into a cubical box, that is to turn the bottom wall with the roughness into a flat plate in the transformed coordinates. (Note that the upper-deck domain is already a cube.) Hence, we define the transformation:

$$x \to \xi: \quad \partial_x(\,) = \partial_\xi(\,) - h\,\partial_\xi F\,\partial_z(\,), \tag{2.57}$$

$$y \to \eta: \quad \partial_y(\,) = \partial_\eta(\,) - h\,\partial_\eta F\,\partial_z(\,), \tag{2.58}$$

$$z_1 - hF(x, y) \to z; \quad \partial_{z_1}(\,) = \partial_z(\,). \tag{2.59}$$

We also define the new velocities, w and W, but keep u_0, U_1, v_0, V_1, p_0, and P_1 unchanged:

$$w \equiv w_0 - h\,\partial_\xi F u_0 - h\,\partial_\eta F v_0, \tag{2.60}$$

$$W \equiv W_1 - h\,\partial_\xi F U_1 - h\,\partial_\eta F V_1. \tag{2.61}$$

Next, we subtract out the upstream Stokes-flow solutions so that the upstream boundary conditions become homogeneous. Therefore, we define the additional transformation:

$$u = u_0 - (1 - \exp(\mathrm{i}^{\frac{3}{4}} S_0^{\frac{1}{2}} z)), \tag{2.62}$$

$$p = p_0 - \mathrm{i} S_0 \xi. \tag{2.63}$$

After substituting all the transformations, the governing equations in the lower deck are

$$\partial_\xi u + \partial_\eta v_0 + \partial_z w = 0, \tag{2.64}$$

$$(\partial_\xi U_1 - \mathrm{i}S_0)\,u + \partial_\eta U_1\, v_0 + \partial_z U_1\, w + U_1\,\partial_\xi u + V_1\,\partial_\eta u + W\,\partial_z u + \partial_\xi p - \partial_{zz} u = -\partial_\xi U_1 + (\partial_\xi U_1 + \mathrm{i}^{\frac{3}{4}} S_0^{\frac{1}{2}} W)\exp(\mathrm{i}^{\frac{3}{4}} S_0^{\frac{1}{2}} z), \tag{2.65}$$

$$(\partial_\eta V_1 - \mathrm{i}S_0)\,v_0 + \partial_\xi V_1\, u + \partial_z V_1\, w + U_1\,\partial_\xi v_0 + V_1\,\partial_\eta v_0 + W\,\partial_z v_0 + \partial_\eta p - \partial_{zz} v_0 = -\partial_\eta V_1(1 - \exp(\mathrm{i}^{\frac{3}{4}} S_0^{\frac{1}{2}} z)), \tag{2.66}$$

$$p = p(\xi, \eta). \tag{2.67}$$

The boundary conditions after the transformation are

$$u = v_0 = w = 0 \quad \text{on} \quad z = 0, \quad \text{for all } \xi \text{ and } \eta, \tag{2.68}$$

$$u, v_0, w \to 0 \quad \text{and/or} \begin{cases} \text{as} & \xi \to -\infty, \quad \text{for all } \eta \text{ and } z \\ \text{as} & |\eta| \to \infty, \quad \text{for all } \xi \text{ and } z. \end{cases} \tag{2.69}$$

Also, as $z \to \infty$ (for all ξ and η), the matching conditions to the main deck require

$$u \to a(\xi, \eta), \tag{2.70}$$

$$\partial_\xi v_0 \to -\frac{\partial_\eta p(\xi, \eta)}{z + hF}, \tag{2.71}$$

where $a(\xi, \eta)$ is defined by asymptotic matching of all thee decks (see (2.78) also). In the above equations, we have scaled out the value of the wall shear of the oncoming, undisturbed boundary layer, λ, by a simple renormalization of variables. The effect of this renormalization is the same as setting $\lambda = 1$ in all the governing equations (see Bodonyi & Duck 1988).

In the upper deck, for the sake of having a uniform notation, we rewrite $(x, y, z_u) \to (\xi, \eta, z_u)$ and also define:

$$\hat{p} = \hat{p}_1 - \mathrm{i}S_0 \xi. \tag{2.72}$$

Analogous to the steady flow, the governing equation with appropriate boundary conditions on the pressure in the upper deck are

$$\partial_{\xi\xi} \hat{P} + \partial_{\eta\eta} \hat{P} + \partial_{z_u z_u} \hat{P} = 0, \tag{2.73}$$

$$\hat{p}(\xi, \eta, z_u) \to 0 \quad \text{as} \quad \begin{cases} \xi \to -\infty & \text{for all } \eta \text{ and } z_u \\ z_u \to \infty & \text{for all } \xi \text{ and } \eta, \end{cases} \tag{2.74}$$

$$\partial_\xi \hat{p} - \mathrm{i}K_\xi \hat{p} \to 0 \quad \text{as} \quad \xi \to \infty \quad \text{for all } \eta \text{ and } z_u, \tag{2.75}$$

$$\partial_\eta \hat{p} - \mathrm{i}K_\eta \hat{p} \to 0 \quad \text{as} \quad \eta \to \pm\infty \quad \text{for all } \xi \text{ and } z_u. \tag{2.76}$$

Also the matching of the solutions in between the decks requires

$$\hat{p}(\xi, \eta, z_u \to 0) = p(\xi, \eta), \tag{2.77}$$

$$\partial_{z_u} \hat{p}(\xi, \eta, z_u \to 0) = \partial_{\xi\xi} a(\xi, \eta). \tag{2.78}$$

The governing equation for the pressure in the upper deck is elliptic and in order to have a well-posed problem, we also need boundary conditions for the unsteady pressure for $\xi \to \infty$ and $\eta \to \pm\infty$. However, this is not a trivial task. Since the governing equations in the lower deck are parabolic, boundary conditions are not needed for them as $\xi \to \infty$. Bodonyi *et al.* (1989) imposed a radiation condition on the outgoing pressure disturbances in the upper deck for their two-dimensional problem. Following their approach we have imposed similar conditions ((2.75) and (2.76)). The wavenumbers, K_ξ and K_η, are computed iteratively from the numerical computations. For example, K_ξ is estimated from the relation (2.75) as

$$(\partial_\xi p)/\mathrm{i}p$$

at some location $\xi_{\text{downstream}}$, reasonably far downstream, and then it is fed back into the numerical computations. The same method is used to evaluate K_η.

3. Numerical method

The method of Bodonyi & Duck (1988) with a slight modification (see Tadjfar 1990) is used to solve the steady-state flow. Also, the method of Bodonyi *et al.* (1989) is generalized to solve the three-dimensional receptivity equations (2.64)–(2.78)

numerically. Following the approach of Smith (1983), to avoid exponential growth of 'departure eigensolutions', we define the skewed shear parameters:

$$\bar{u} = \partial_\xi u + \partial_\eta v_0, \quad \bar{w} = \partial_\xi w, \quad \bar{e} = [\partial_{\xi\xi} + \partial_{\eta\eta}]\, p(\xi, \eta). \tag{3.1}$$

Furthermore, define a new function,

$$\int_{-\infty}^{\xi} b(x, \eta)\, \mathrm{d}x = \partial_\xi a(\xi, \eta). \tag{3.2}$$

Using the above definitions and differentiating the governing equations (2.64)–(2.66), it can be shown that

$$\partial_\xi \bar{u} + \partial_z \bar{w} = 0, \tag{3.3}$$

$$-\mathrm{i}S_0 \bar{u} + U\partial_\xi \bar{u} + W\partial_z \bar{u} + \partial_z U\bar{w} + \bar{e} - \partial_{zz}\bar{u} = rh, \tag{3.4}$$

where, rh is given by

$$\begin{aligned} rh = &-(1+u)(\partial_{\xi\xi} U + \partial_{\xi\eta} V) \\ &+ (\partial_{\xi\xi} U + \partial_{\xi\eta} V + \mathrm{i}^{\frac{3}{4}} S_0^{\frac{1}{2}} \partial_\xi W) \exp(\mathrm{i}^{\frac{3}{4}} S_0^{\frac{1}{2}}) - w(\partial_{z\xi} U + \partial_{z\eta} V) \\ &- \partial_\xi W \partial_z u - 2\partial_\xi U \partial_\xi u - 2\partial_\eta V \partial_\eta v_0 - 2\partial_\xi V \partial_\eta u - 2\partial_\eta U \partial_\xi v_0 \\ &- \partial_\eta W \partial_z v_0 - \partial_z V \partial_\eta w - v(\partial_{\eta\xi} U + \partial_{\eta\eta} V) - V(\partial_{\eta\xi} u + \partial_{\eta\eta} v_0), \end{aligned} \tag{3.5}$$

and the boundary conditions, (2.68) and (2.69), transform to

$$\bar{u} = \bar{w} = 0 \quad \text{on} \quad z = 0, \tag{3.6}$$

$$\bar{u}, \bar{w}, \bar{e} \to 0 \quad \text{as} \quad \xi \to -\infty. \tag{3.7}$$

Also, as $z \to \infty$, we can approximate the momentum equation (3.4):

$$\begin{aligned} (\bar{w} + \bar{e}) \to \Bigg(&\mathrm{i}S_0 \int_{-\infty}^{\xi} b(x, \eta)\, \mathrm{d}x - U(z \to \infty)\, b(\xi, \eta) \\ &- 2\partial_\xi U(z \to \infty)\, \partial_\xi u - \partial_{\xi\xi} U(z \to \infty)\, (1+u) \Bigg). \end{aligned} \tag{3.8}$$

Similarly for the upper-deck pressure, we define

$$\hat{e}(\xi, \eta, z_\mathrm{u}) = \partial_{\xi\xi} \hat{p}(\xi, \eta, z_\mathrm{u}) + \partial_{\eta\eta} \hat{p}(\xi, \eta, z_\mathrm{u}). \tag{3.9}$$

Therefore, the governing equation (2.73) in the upper deck becomes

$$\partial_{\xi\xi} \hat{e} + \partial_{\eta\eta} \hat{e} + \partial_{z_\mathrm{u} z_\mathrm{u}} \hat{e} = 0, \tag{3.10}$$

and the boundary conditions (2.74)–(2.76) become

$$\hat{e}(\xi, \eta, z_\mathrm{u}) \to 0 \quad \text{as} \quad \xi \to -\infty, z_\mathrm{u} \to \infty, \tag{3.11}$$

$$\partial_\xi \hat{e} \to \mathrm{i}K_\xi \hat{e}(\xi, \eta, z_\mathrm{u}) \quad \text{as} \quad \xi \to \infty, \tag{3.12}$$

$$\partial_\eta \hat{e} \to \mathrm{i}K_\eta \hat{e}(\xi, \eta, z_\mathrm{u}) \quad \text{as} \quad \xi \to \pm\infty. \tag{3.13}$$

We also need the matching conditions, (2.77) and (2.78), to close the problem:

$$\hat{e}(\xi, \eta, z_\mathrm{u} \to 0) = \bar{e}(\xi, \eta), \tag{3.14}$$

$$\partial_{z_\mathrm{u}} \hat{e}(\xi, \eta, z_\mathrm{u} \to 0) = \partial_{\xi\xi} b(\xi, \eta) + \partial_{\eta\eta} b(\xi, \eta). \tag{3.15}$$

The receptivity problem is solved by the same technique as utilized for the steady problem. Following Bodonyi & Duck (1988) an iterative multi-sweep technique,

using forward marching in a quasi two-dimensional manner is used to solve the above equations. The ξ, η, z and z_u axes are discretized using the indices $i = 0, 1, 2, \ldots, nx-1, nx, j = 0, 1, 2, \ldots, ny-1, ny$, $k = 1, 2, 3, \ldots, n-1, n$, and $q = 1, 2, 3, \ldots, m-1, m$ respectively. The grid spacings are given by $\Delta\xi$, $\Delta\eta$, Δz, and Δz_u. The governing equations for the receptivity problem are differenced using a second-order-accurate scheme. The mesh is the same as the one used for the steady-state problem and the results of the steady-state solution, U, V, and W, are stored for all mesh points, since they are needed to evaluate the coefficients in the unsteady problem. Flow properties and their derivatives are centrally differenced about the node at $(i-\frac{1}{2}, j$ and $k)$. This leads to a system of equations along a line perpendicular to the wall at any node (i,j). The above sparse system is easily solved using standard Gaussian elimination to obtain $\bar{u}$, $\bar{w}$, $\bar{e}$, b and $\hat{e}$ for all k and q along that line.

This procedure is started at the node $i = 1$ and $j = 0$, where $i = 0$ is the upstream boundary, $\xi = \xi_{-\infty}$, at which point the solution to the unsteady boundary layer is imposed. Also, $j = 0$ is the location of the line of symmetry, where the usual symmetry conditions are applied. The governing equations in both the lower and upper decks are solved simultaneously over the entire range of the normal directions, z and z_u. After the solution is found along this line, normal to the wall, the procedure is marched forward in ξ until the entire (ξ, η)-plane is covered. The process is then repeated at all the other η-locations (i-fastest) to obtain this iteration of the solution over the entire domain. Once the new values of $\bar{u}$, $\bar{w}$, $\bar{e}$, b and $\hat{e}$ are found over the entire domain, the definition of $\bar{e}$ is used to solve for the new values of unsteady pressure. The above Poisson equation, (3.1), is solved using the successive-over-relaxation technique with $\omega_{SOR} = 1.6$. Having found the pressure values at this global iterative step, we march the original η-momentum equation (2.66) in ξ to calculate new values for v_0. This results in a tri-diagonal system of equations which can easily be solved using the Thomas algorithm. Finally, the remaining velocity components are determined by integrating the skewed shears, (3.1), to get back the primitive variables.

All the above steps constitute one global iteration. The solution (all the flow variables in their primitive form) obtained after one iteration is used as an initial guess for the next iterative step. This process is continued until global convergence is attained on the disturbance streamwise velocity u. That is,

$$\max\left[u^{j^k}_{u_{i_{\text{new}}}} - u^{j^k}_{u_{i_{\text{old}}}}\right] < \hat{\epsilon} \quad \text{for all } i, j, k,$$

where $\hat{\epsilon}$ is a small number, usually in the order of 10^{-5}. It should also be noted that for regions of reversed flow the parabolic direction of the flow changes locally so that the forward-marching scheme used here becomes unstable. To overcome this difficulty the approximation suggested by Reyhner & Flugge-Lotz (1968) is implemented in the backflow regions. As shown by Williams (1974), this approximation is only valid and has little effect on the solution if the reversed flow velocities are small in magnitude.

4. Numerical results

Since we are interested in a general study of the problem, the choice of the hump shape is not crucial. To be consistent with prior work, Bodonyi & Duck (1988), Bodonyi *et al.* (1989), we use the same hump shape as given below (see figure 2):

$$F(x, y) = \exp\left[-x^2 - y^2\right]. \tag{4.1}$$

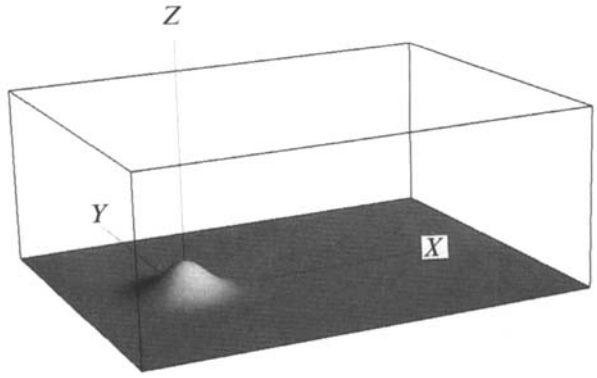

FIGURE 2. Computational domain and the hump shape as given by equation (4.1).

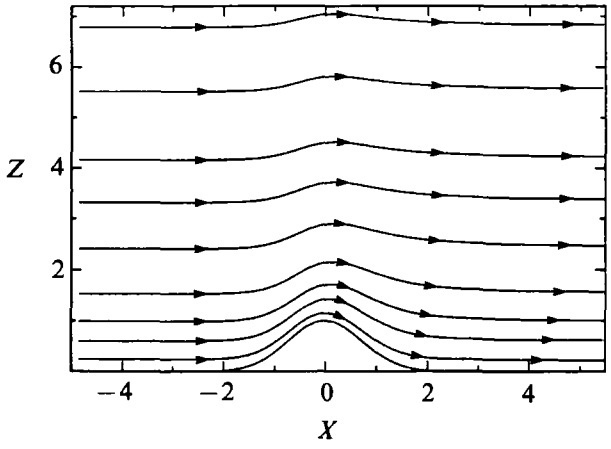

FIGURE 3. Flow streamlines at the plane of symmetry; $Y = 0$ at hump height $h = 1.0$.

In the steady-flow computations the following values were used for the parameters: in the streamwise direction $\Delta X = 0.10$, $-5.0 < X < 10.0$; along the lateral direction we have $\Delta Y = 0.10$, $0 < Y < 5.0$, and in the normal direction within the lower-deck region $\Delta Z = 0.10$ and $0 < Z < 9.0$. These values correspond to using 151, 50, and 90 points in the X-, Y-, and Z-directions, respectively. In the upper-deck region the same values were used for ΔX and ΔY while $\Delta Z_u = 0.10$ and $0 < Z_u < 6.0$, corresponding to the same number of grid points in the X- and Y-directions as in the lower-deck problem, with 60 points used in the Z-direction.

For the height, $h = 1.0$, the boundary layer is displaced over the hump without separation. This is clearly evident in the flow streamlines at the plane of symmetry, $Y = 0$, presented in figure 3. Figure 4 presents the contour plot of the steady-pressure perturbations imposed across the boundary layer due to the hump's presence. As can be seen, the flow is first slowed ahead of the hump, giving rise to the pressure peak there, and then the flow is accelerated over the hump to reach a minimum pressure point at the tip of the hump. Eventually these steady-pressure perturbations disappear downstream of the hump. The negative of the displacement thickness, $A(X, Y)$ as defined by (2.28), is a measure of the slope of the flow over the hump and is presented in figure 5. A small wake region is evident in the above figure, which

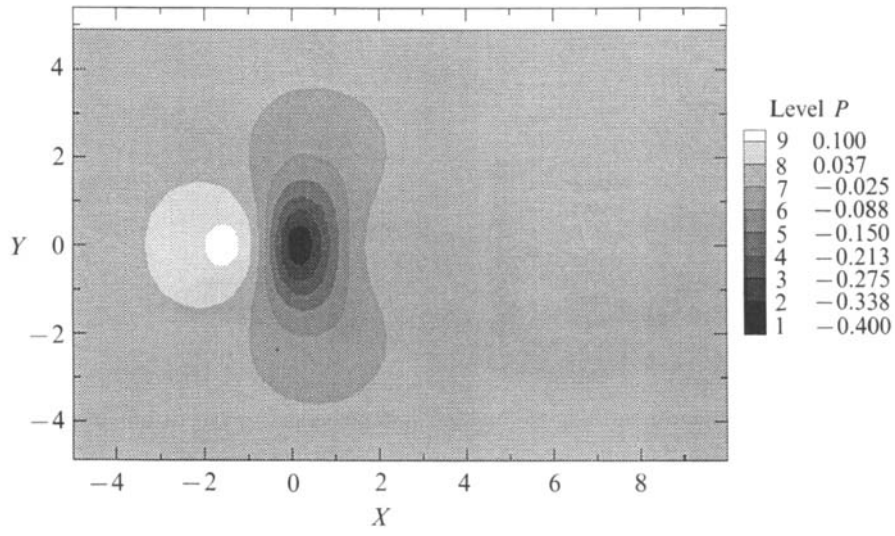

FIGURE 4. Contour plot of steady pressure for the hump with $h = 1.0$.

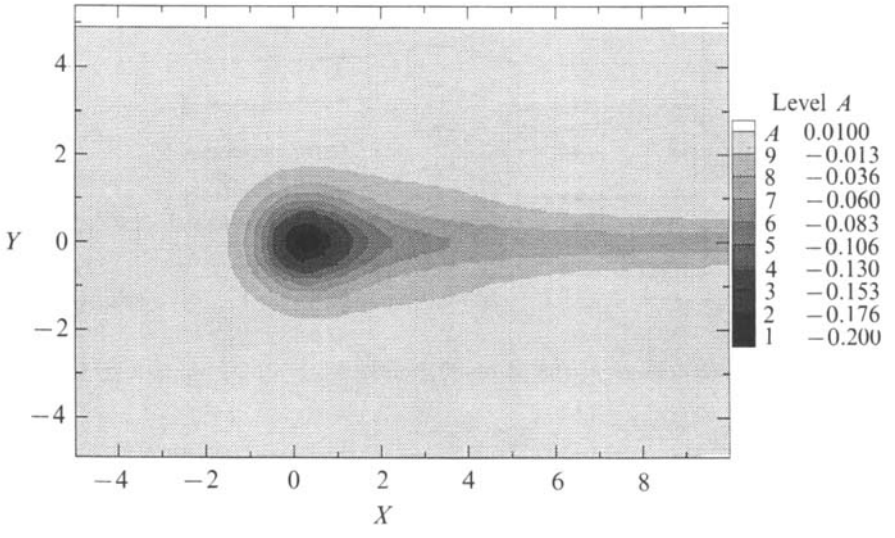

FIGURE 5. Contour plot of $A(X, Y)$ for the hump with $h = 1.0$.

extends out of the computational domain. Further studies of the steady-state problem can be found in Tadjfar (1990).

4.1 *Receptivity of the laminar boundary layer*

The main goal of this study is to investigate the receptivity of a laminar boundary layer to the local interaction of free-stream disturbances with a small three-dimensional roughness element. Without the hump, the free-stream disturbances, to the first order, produce the classical Stokes flow near the wall in the lower deck. In (2.62) and (2.63), we subtracted this uniform Stokes flow out of our solution. Hence, in the hump's absence the disturbance flow is zero everywhere.

In our disturbance-flow computer program, all the flow variables are complex valued and all the steady-flow variables are also needed to evaluate the coefficients. Therefore, owing to computer-storage limitations, a coarser mesh than the one used

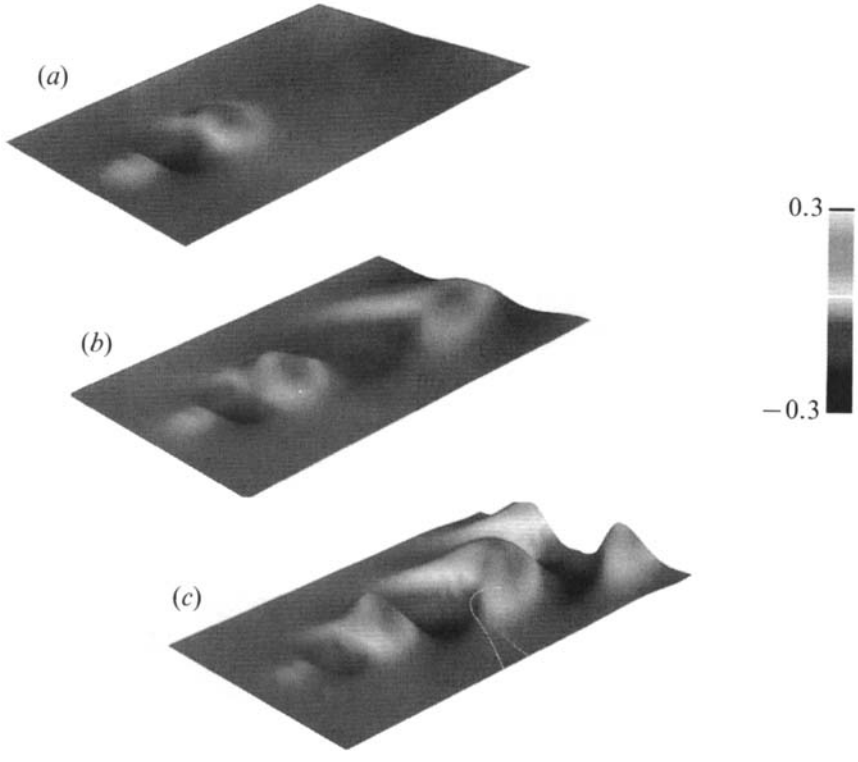

FIGURE 6. Surface plots of T–S wave pressure for (*a*) $S_0 = 1.0$, (*b*) 2.0, and (*c*) 3.0 at time $t = 0$.

to evaluate the steady-state flow field is necessary. However, this restriction is not crucial. For convenience, we have replaced ξ, η, and z_l by X, Y, and Z, respectively. Furthermore, the following values were used for the parameters: in the streamwise direction $\Delta X = 0.30$, $-3.6 < X < 11.4$; along the lateral direction we have $\Delta Y = 0.20$, $0 < Y < 6.0$; and in the normal direction within the lower-deck region $\Delta Z = 0.30$ and $0 < Z < 6.3$. These values correspond to using 50, 30, and 21 points in the X-, Y-, and Z-directions, respectively. In the upper-deck region the same values were used for ΔX and ΔY while $\Delta Z_u = 0.20$ and $0 < Z_u < 3.2$, corresponding to the same number of grid points in the X- and Y-directions as in the lower-deck problem with 16 points used in the Z_u direction.

The effect of using this mesh on these computations is examined by computing the results for $S_0 = 1.0$ with different mesh sizes. In separate numerical calculations the number of points in one direction is doubled, with all the other parameters unchanged. This is repeated for all three directions in the lower deck and the normal direction in the upper deck. The range of the mesh is also extended in all the directions in separate computations. No noticeable changes (less then one percent) in the results are observed. Hence, it is concluded that the above mesh is sufficient for studying the disturbance-flow field over the given hump. For all these computations the steady flow field is calculated on the finer mesh given previously. For the steady-flow computations, the upstream influence of the hump's presence required that the upstream boundary conditions be applied at $X = 5.0$. However, in the disturbance-flow computations, the upstream propagation of the disturbance decays more rapidly, therefore, making it possible to apply the upstream boundary conditions at $X = -3.6$ (thereby lowering the computational costs).

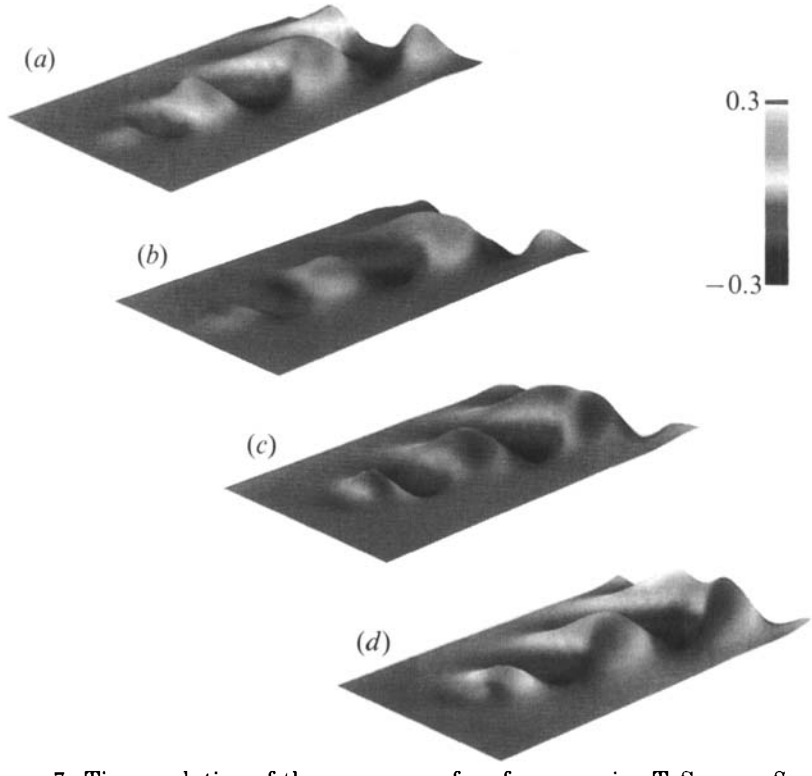

FIGURE 7. Time evolution of the pressure surface for a growing T–S wave, $S_0 = 3.0$, at times (*a*) $t = 0$, (*b*) $\pi/2$ and (*c*) $3\pi/2$.

Guided by the two-dimensional studies of Bodonyi *et al.* (1989), we expect the crucial parameter to be the scaled Strouhal number, S_0. Therefore, we study the effect of varying the Strouhal number on the disturbance flow as it is convected downstream. For all order-one scaled Strouhal numbers, the interaction of the hump and the free-stream disturbances introduces a spectrum of all spatial disturbances in the boundary layer around the hump. For $S_0 = 1.0$, this initial kink decays rapidly as it moves downstream. As the Strouhal number is increased, the rate of attenuation decreases. About $S_0 = 2.0$ the total energy introduced by the interaction stays constant and is only spread spanwise. As the Strouhal number is further increased, the initial kink is amplified as it moves downstream. This can be seen in figure 6, which shows the disturbance-pressure surfaces for $S_0 = 1.0$, 2.0, and 3.0 at time $t = 0$. Pressure is a good variable to follow the disturbance motion downstream, since it is uniform across the boundary layer to this order in the asymptotic expansions. For $S_0 = 3.0$ the disturbance is growing in a wedge shape extending downstream of the hump. The wave motion is periodic, equations (2.47) and (2.48), and is repeated every $\Delta t = 2\pi$. This time evolution is shown in figure 7. The spatial and temporal evolutions are related; the second and third crests seen at time $t = 0$ are simply the first crest having been amplified as it moves downstream at times $t = 2\pi$ and 4π respectively.

Similar structures are also evident in all other flow quantities. However, disturbance velocities are a function of the normal direction and exhibit variations along the Z-axis. This can be seen by comparing the u-velocity contours near the outer edge of the lower deck to the values near the wall (see figures 8 and 9). $a(X, Y)$

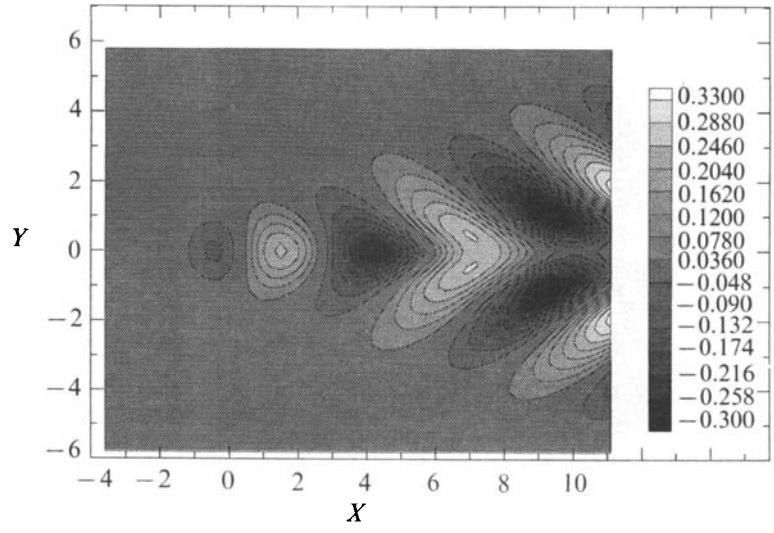

FIGURE 8. Contour plot of $a(x, y, t)$ representing u-velocity near the outer edge of the lower deck for $S_0 = 3.0$ at time $t = 0$.

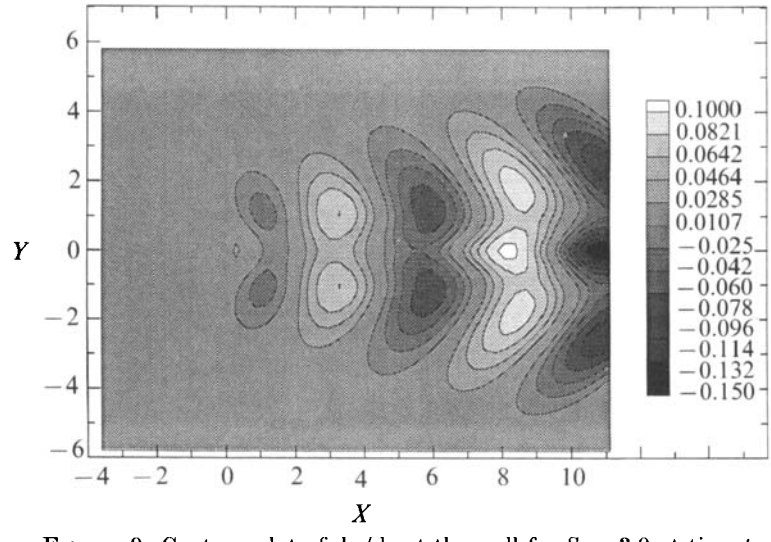

FIGURE 9. Contour plot of $\mathrm{d}u/\mathrm{d}z$ at the wall for $S_0 = 3.0$ at time $t = 0$.

can be interpreted as the limiting value of the streamwise disturbance velocity u, at the outer edge of the lower deck, by equation (2.70). Streamwise wall-shear, $\mathrm{d}u/\mathrm{d}\tilde{z}\ (x, y, t; z = 0)$, represents the u-velocity field near the wall. Contours of $a(X, Y)$ are similar to the pressure contours shown in figures 6 and 7 with a phase shift. The time-averaged amplitude of u-velocity, u_{rms}, at the outer edge of the lower deck is given by the modulus $|a_c(x, y)|$. A contour map of u_{rms} amplitude is presented in figure 10.

To study the growth or decay of the disturbance motion as it is convected downstream, we need to define a measure of the disturbance energy. We use the disturbance pressure owing to its lack of dependency on the normal direction, Z, which makes it valid across the boundary layer and not just the lower deck. By

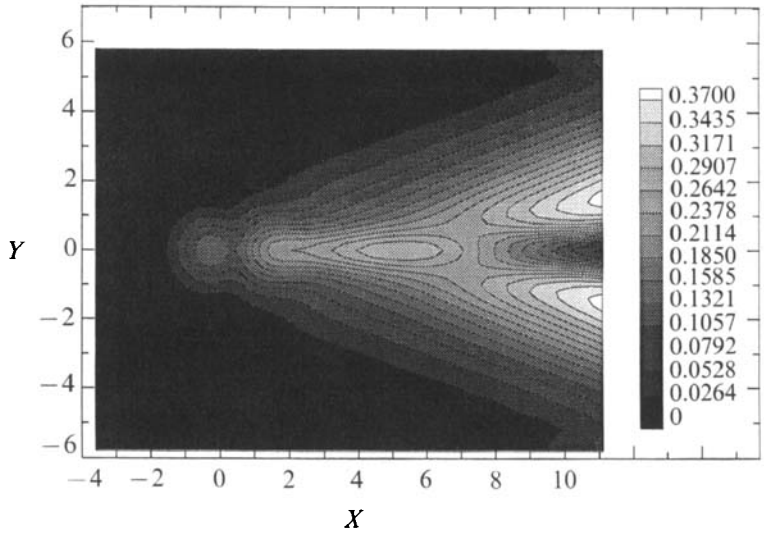

FIGURE 10. Contour map of $|a_c(x, y)|$ representing u_{rms} near the outer edge of the lower deck for $S_0 = 3.0$.

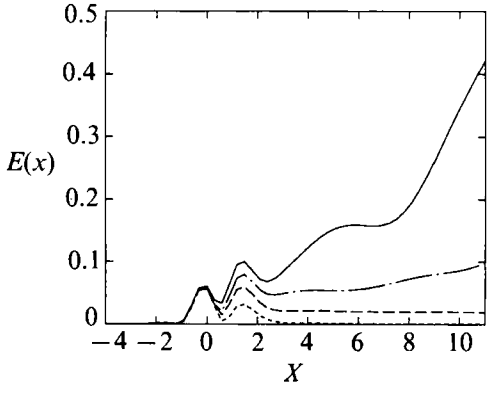

FIGURE 11. Energy function, $E(x)$, for $S_0 = 1.0$ (----), 2.0, (– – –), 2.5, (—·—), and 3.0 (——) at time $t = 0$.

integrating some representation of disturbance energy, which we define as the square of the time-averaged amplitude of pressure, across the spanwise direction, we define an energy function:

$$E(x) = \int_{-\infty}^{\infty} |p_c(x, y)|^2 \, dy. \tag{4.2}$$

Energy functions for different Strouhal numbers are presented in figure 11. The effect of Strouhal number on growth or decay of the internalized wave motion is evident in the energy function plots. The value of the energy function at the roughness location, $E_0 = E(x = 0)$, can be seen as a measure of receptivity. This is the initial amount of energy internalized by the receptivity mechanism at the roughness location. E_0 is related to the square of δ, the ratio of the free-stream disturbance strength to free-stream velocity, by (2.7).

Amplification curves for $\ln(E/E_0)$ versus X for various Strouhal numbers are plotted in figure 12. The energy function amplitudes are normalized by E_0 so the

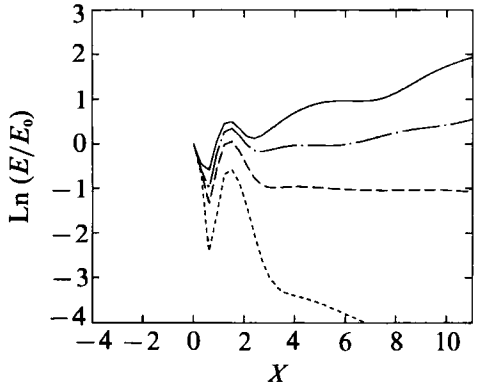

FIGURE 12. Normalized amplification curves of the energy function for $S_0 = 1.0$ (----), 2.0, (– – –), 2.5, (—·—), and 3.0 (——) at time $t = 0$.

amplification curves have a zero value at the input location. From the amplification curves we can determine the growth rate of the T–S waves generated using the formula:

$$\alpha(x) = -\frac{1}{2}\frac{\mathrm{d}(\ln(E/E_0))}{\mathrm{d}x}. \tag{4.3}$$

The factor $-\frac{1}{2}$ is used to be able to compare the computed growth rates to that of a two-dimensional T–S wave, K_1, as found in the linearized analysis of Duck (1985). The calculated growth rates and their two-dimensional counterparts are plotted in figure 13. The computed values approach a value slightly higher than the ones calculated by the linearized analysis. This is also evident in that the computed neutral Strouhal number, $S_0 = 2.0$, is lower than that calculated by the linearized analysis for two-dimensional T–S waves, $S_0 = 2.29\ldots$.

4.2. *Concluding remarks*

In the absence of any roughness element, the free-stream disturbances, to the first order, produce the classical Stokes flow, in the thin Stokes layer near the wall (on the order of our lower deck). However, with the introduction of a small three-dimensional roughness element, the interaction between the hump and the Stokes flow introduces a spectrum of all spatial disturbances inside the boundary layer. For values of $S_0 < 2.0$, this initial kink decays rapidly. As $S_0 = 2.0$ is approached the rate of this attenuation decreases. At $S_0 = 2.0$ the total wave energy stays constant and is only spread spanwise as it moves downstream (see figures 6, 11, and 12). For higher values of $S_0 > 2.0$, T–S wave energy is amplified in a wedge-shaped region, 15°–18° to the basic-flow direction, extending downstream of the hump. However, the maximum amplification occurs along a ray of 7.5°–9°, at the wedge half angle, from the basic-flow direction (see figures 8, 9, and 10). The existence of this wedge-shaped amplification domain or the oblique maximum amplification direction cannot be explained by relating them to the steady-flow perturbations in the wake region downstream of the hump (see figure 5). At the exit boundary, $X = 11.0$, the steady-flow wake region extends to $Y = \pm 0.5$. However, the T–S wave peak amplitudes are at $Y = \pm 1.5$ to ± 2.0 depending on the Z-location.

The near-field region downstream of the hump is influenced by the wake of the hump. Therefore, the instability waves generated by the hump are not truly the

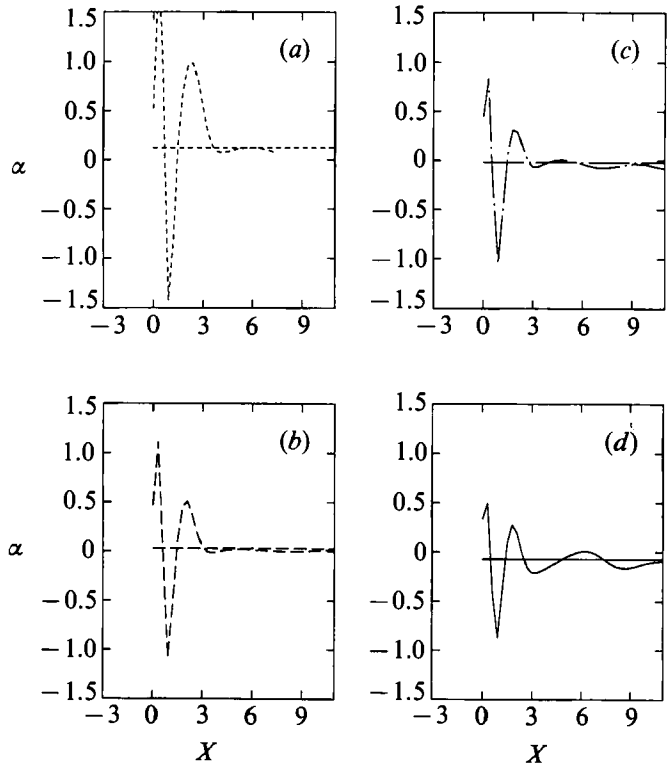

FIGURE 13. Computed growth rates, $\alpha(x)$, *vs.* the values from linearized analysis of Duck (1985), K_1, for the two-dimensional T–S wave where: (*a*) $K_1(S_0 = 1.0) = 0.12067$; (*b*) $K_1(S_0 = 2.0) = 0.03227$; (*c*) $K_1(S_0 = 2.5) = -0.02194$; (*d*) $K_1(S_0 = 3.0) = -0.07472$.

classical T–S waves. However, these instability waves approach the classical T–S waves asymptotically further downstream. The critical Strouhal number in our study is near $S_0 = 2.0$, which is just below the value $S_0 = 2.29\ldots$, describing the lower branch of the neutral-stability curve for the Blasius profile. Also, the computed growth rates approach a value slightly higher than the ones calculated by the linearized analysis for two-dimensional T–S waves (see figure 13).

In this analysis, we have considered the infinite-wavelength uniform pulsation of the free stream corresponding to a plane acoustic field in an incompressible flow. Goldstein & Hultgren (1989) point out that in physical flows the inviscid free-stream disturbances have the convective wavelength U_∞^*/f, which in the high-Reynolds-number limit is of $2\pi O(\epsilon^2)$ (very long compared with the T–S wavelength). Hence, the interaction of much longer oscillations, of $2\pi O(\epsilon^2)$ or larger, in the free stream with a small three-dimensional roughness element have generated much shorter T–S waves, of $O(\epsilon^3)$, inside the laminar boundary layer. Accumulation of these three-dimensional patches of T–S waves generated by the local receptivity mechanism at every small surface-roughness location may explain one source of natural transition.

Gilev & Kozlov (1984) used a thin rectangular vibrating film (188 × 28 mm) mounted on the surface to introduce harmonic disturbances into the flow. In their experiment the disturbances are directly inputted into the boundary layer at the wall. In our analysis, instability waves are generated due to the acoustic-roughness interaction. However, there are enough similarities in the results that may be compared qualitatively. They observed a local maximum of the disturbance

amplitude above the vibrating film. The magnitude of this initial amplitude was practically independent of the frequency of the oscillation and only its evolution further downstream was influenced by the input frequency. This same phenomenon can be observed in our results in the value of the energy function above the roughness element at $X = 0$ (see figure 11). A rapid attenuation of disturbance energy was seen upstream of the vibrator irrespective of the oscillation frequency. In addition, they reported the existence of a local minimum in the disturbance amplitude just downstream of the vibrator. The introduced instability wave evolved into a T–S wave further downstream. (This was evident in the reported profiles of $u'_{\rm rms}$ and the phase of the disturbance across the boundary layer.) All the above-mentioned effects can be seen in the energy function plot of the instability wave, induced by the roughness–acoustic interaction, in our analysis. In fact, our figure 11 is very similar to the figure 6 of Gilev & Kozlov (1984).

The authors are grateful to Ohio Supercomputer Center for providing computer time on the Cray Y-MP supercomputer.

REFERENCES

BODONYI, R. & DUCK, P. 1988 A numerical method for treating strongly interactive three-dimensional viscous–inviscid flows. *Comput. Fluids* **16**, 279–290.

BODONYI, R., WELCH, P., DUCK, P. & TADJFAR, M. 1989 A numerical study of the interaction between unsteady free-stream disturbances and localized variations in surface geometry. *J. Fluid Mech.* **209**, 285–308.

DUCK, P. 1985 Laminar flow over unsteady humps: the formation of waves. *J. Fluid Mech.* **160**, 465–498.

DUCK, P. & BURGGRAF, O. 1986 Spectral solutions for three-dimensional triple-deck flow over surface topography. *J. Fluid Mech.* **162**, 1–22.

GASTER, M. 1975 A theoretical model of a wavepacket in the boundary layer on a flat plate. *Proc. R. Soc. Lond.* A **347**, 271–289.

GASTER, M. 1985 On wave packets in laminar boundary layers. *IUTAM Symp., Laminar-Turbulent Transition, Novosibirsk, USSR* (ed. V. V. Kozlov). Springer.

GASTER, M. & GRANT, I. 1975 An experimental investigation of the formation and development of wavepacket in a laminar boundary layer. *Proc. R. Soc. Lond.* A **347**, 253–269.

GILEV, V. M., KACHANOV, Y. S. & KOZLOV, V. V. 1981 Development of a spatial wave packet in a boundary layer. *Preprint* 34-81, Inst. of Theoretical and Appl. Math., USSR Acad. Sci., Novosibirsk.

GILEV, V. M. & KOZLOV, V. V. 1984 Excitation of Tollmien–Schlichting waves in the boundary layer on a vibrating surface. *Zh. Prik. Mekh. Tekh. Fiz.*, No. 6, p. 73.

GOLDSTEIN, M. 1983 The evolution of Tollmien–Schlichting waves near a leading edge. *J. Fluid Mech.* **127**, 59–81.

GOLDSTEIN, M. 1985 Scattering of acoustic waves in Tollmien–Schlichting waves by a small streamwise variations in surface geometry. *J. Fluid Mech.* **154**, 509–529.

GOLDSTEIN, M. & HULTGREN, L. S. 1987 A note on the generation of Tollmien–Schlichting waves by sudden surface curvature change. *J. Fluid Mech.* **181**, 519–525.

GOLDSTEIN, M. & HULTGREN, L. S. 1989 Boundary layer receptivity to long-wave free-stream disturbances. *Ann. Rev. Fluid Mech.* **21**, 137–166.

HERBERT, TH. & BODONYI, R. 1989 Studies of transition in boundary layers. *AIAA Meeting, Reno, AIAA*-89-0034.

KACHANOV, Y. S. 1985 Development of spatial wave packets in a boundary layer. *IUTAM Symp., Laminar-Turbulent Transition, Novosibirsk, USSR* (ed. V. V. Kozlov). Springer.

MACK, L. 1984 Boundary-layer linear stability theorem. *AGARD Special Course on Stability and Transition.*

MACK, L. M. & KENDALL, J. M. 1983 Wave pattern produced by a localized harmonic source in a Blasius boundary layer. *AIAA Meeting, Reno, AIAA*-83-0046.

MESSITER, A. F. 1970 Boundary layer flow near the trailing edge of a flat plate. *SIAM J. Appl. Math.* **18**, 241–257.

NEILAND, V. Y. 1969 Towards a theory of separation of the laminar boundary layer in a supersonic stream. *Izv. Akad. Nauk SSSR, Mekh. Zhidk. Gaza.*, pp. 53–57 (Transl. in *Fluid Dyn.* **4**, 33–35).

RESHOTKO, E. 1976 Boundary-layer stability and transition. *Ann. Rev. Fluid Mech.* **8**, 311–349.

RESHOTKO, E. 1984 *Environment and receptivity. AGARD Rep.* 709.

REYHNER, T. A. & FLUGGE-LOTZ, I. 1968 *Intl J. Nonlinear Mech.* **3**, 173.

ROSENHEAD, L. 1963 *Laminar Boundary Layers.* Oxford University Press.

SMITH, F. T. 1979 On the non-parallel flow stability of the Blasius boundary layer. *Proc. R. Soc. Lond.* A **366**, 91–109.

SMITH, F. T. 1982 On the high Reynolds number theory of laminar flows. *IMA J. Appl. Maths* **28**, 207–281.

SMITH, F. T. 1983 Properties, and a finite-difference approach, for interactive three-dimensional boundary layers. *UTRC*-83-46.

SMITH, F. T. 1986 Steady and unsteady boundary-layer separation. *Ann. Rev. Fluid Mech.* **18**, 197–220.

STEWARTSON, K. 1974 Multistructured boundary layers on flat plates and related bodies. *Adv. Appl. Mech.* **14**, 145–239.

STEWARTSON, K. & WILLIAMS, P. G. 1969 Self-induced separation. *Proc. R. Soc. Lond.* A **312**, 181–206.

TADJFAR, M. 1990 Receptivity of a laminar boundary layer to the interaction of a three-dimensional roughness element with time-harmonic free-stream disturbances. Ph.D. dissertation, Dept. of Aero. & Astro. Eng., The Ohio State Univ.

WILLIAMS, P. G. 1974 *Proc. 4th Intl Conf. on Num. Methods in Fluid Dynamics.*